Isovector properties of finite nuclei: constraints from neutron stars observations

Manolis Divaris[1,*], *Alkiviadis* Kanakis-Pegios[1,**], and *Charalampos* Moustakidis[1,***]

[1]Department of Theoretical Physics, Aristotle University of Thessaloniki, 54124 Thessaloniki, Greece

Abstract. The nuclear symmetry energy plays a crucial role in the structure of finite nuclei and the bulk properties of neutron stars. However, its values at high densities are highly uncertain, and the corresponding experimental data have large errors. One way to determine or at least estimate these high-density values is through neutron star observations. Recently, observations of gravitational waves from binary neutron star mergers have provided useful information on their radius and tidal deformability, which are directly related to the symmetry energy. This work attempts to use recent observations to constrain the structure of finite nuclei. Specifically, we parameterize the equation of state (EoS) describing asymmetric and symmetric nuclear matter using the parameter $\eta = (K_0 L^2)^{1/3}$, where K_0 is the incompressibility and L is the slope parameter, The parameter η regulates the stiffness of the EoS, and we expect its values to affect both finite nuclei and neutron star properties, especially given the important role of isovector interactions. It is natural to expect that constraints on η for finite nuclei will also imply constraints on neutron star properties and vice versa. In light of the above, we propose a simple yet self-consistent method to simultaneously examine the effects of η on the properties of finite nuclei and neutron stars. We found constraints on these systems by combining recent experimental data (PREX-2) and observational data from the LIGO and Virgo detectors.

1 Introduction

The Nuclear Symmetry Energy (NSE) is crucial for understanding both neutron-rich finite nuclei and neutron stars (see Refs. [1–10] and references therein). It reflects the isovector nature of nuclear forces and varies significantly with baryonic density. While terrestrial experiments help reduce uncertainty at low densities akin to finite nuclei, the values of NSE at high densities remain completely uncertain with substantial empirical errors. Both theoretical and experimental efforts focus on correlating two key parameters of the NSE: the slope parameter L and its value J on the saturation density n_0. These parameters are studied in relation to diverse nuclear properties, including masses, neutron skin thickness, dipole polarizability, resonance energies, heavy-ion collisions, and isobaric analog states. Moreover, NSE plays a crucial role in shaping neutron star properties such as radius, maximum mass, crust-core transition density affecting crust thickness, thermal relaxation time, neutrino cooling processes, and reaction rates crucial for the astrophysical r-process. Existing equations of state (EOS) typically focus separately on either finite nuclei or neutron star structures, rarely integrating both systems in a self-consistent manner. However, when achieved, such integration reveals direct dependencies between microscopic properties governing finite nuclei and macroscopic properties influencing neutron stars, owing to their common origins. Alternatively, researchers often employ diverse approaches and nuclear models for nuclei and neutron stars, correlating their properties through systematic studies documented in the literature.

This study aims to explore these relationships in a self-consistent manner using a unified nuclear model to analyze isovector properties across both finite nuclei and neutron stars. In this paper, we utilize data from the PREX-2 experiment regarding the neutron skin thickness of ^{208}Pb (where $\Delta R_{\rm skin} = 0.283 \pm 0.071$ fm) [11, 12]. The thickness values observed in this experiment are notably larger compared to those from other similar experiments (see for example the results of the CREX Collaboration where found the value $\Delta R_{\rm skin} = 0.121 \pm 0.026$ fm for the case of ^{48}Ca [13]), imposing significant constraints on the slope of the nuclear symmetry energy and necessitating a stiff EoS, at least for densities near the saturation density. Expanding on prior work (see Ref. [14]) that concentrated on finite nuclei, this research extends to encompass investigations into neutron star properties as well. Building on the approach from previous studies (Refs. [15, 16]), we parameterize the EoS for symmetric and asymmetric nuclear matter using the parameter $\eta = (K_0 L^2)^{1/3}$, where K_0 is the incompressibility and L the slope parameter. The parameter η serves as a regulator that controls the stiffness of the EoS. Our computational procedure can be summarized as follows: Firstly, we constructed a self-consistent density functional method based on the parametrization described earlier. This method is designed to efficiently analyze the effects of symmetry energy on the isovector

*e-mail: edivar@auth.gr
**e-mail: alkanaki@auth.gr
***e-mail: moustaki@auth.gr

© The Authors, published by EDP Sciences. This is an open access article distributed under the terms of the Creative Commons Attribution License 4.0 (https://creativecommons.org/licenses/by/4.0/).

structure properties of medium and heavy neutron-rich nuclei. Secondly, we utilize these equations of state to investigate both the structure and bulk properties of neutron stars. This approach offers the advantage of employing the same energy density functional to study both finite nuclei and neutron stars. The key parameter η serves as a crucial link connecting the microscopic properties of nuclei to the macroscopic properties of neutron stars. Any experimental limitations affecting the properties of finite nuclei will consequently influence corresponding properties of neutron stars, and vice versa. For more details on the theory of the proposed model, computational methodology and results, one can look at the extensive work [17].

The structure of the paper is as follows: Section 2 introduces the model used to study both finite nuclei and neutron stars. Section 3 is focused on presenting the results and providing relevant discussion. Finally, in section 4 we conclude the investigation providing our final remarks.

2 The model

2.1 Finite Nuclei

The corresponding energy density $\mathcal{E} = nE$, which is the key quantity in the present study and essentially serves to *bridge* the properties of finite nuclei and nuclear matter (neutron star matter) reads

$$\begin{aligned}\mathcal{E}_b(n,\alpha) &= E_0 n + \frac{K_0}{18n_0^2} n\,(n-n_0)^2 \\ &+ \left(J + \frac{L}{3n_0}(n-n_0)\right) n\alpha^2 \end{aligned} \tag{1}$$

where $\alpha = (n_n - n_p)/n$ is the asymmetry parameter, with n_n and n_p the number densities of neutrons and protons respectively and $n_0 = 0.16$ fm^{-3} is the saturation density. Moreover $E_0 = E(n_0, 0)$ is the energy per particle at n_0, K_0 is the incompressibility and $S(n)$ is the symmetry energy. In particular, the nuclear symmetry energy $S(n)$ can be developed in a series around the saturation density

$$S(n) = J + \frac{L}{3n_0}(n-n_0) + \cdots \tag{2}$$

where $J = S(n_0)$. The slope parameter L is related to the first derivative of the NSE according to the definition

$$L = 3n_0 \left(\frac{dS(n)}{dn}\right)_{n=n_0} \tag{3}$$

Expression (1) is a very good approximation for densities close to the saturation density with appropriate parameterization of the parameters K_0, J and L. Although it is questionable whether it is plausible at high densities involving neutron star matter, there are two reasons to support its extension to higher densities. The first one is that the second-order expansion with respect to the asymmetry parameter α is a good approximation even in cases where the fraction of neutrons is dramatically larger than that of protons (this is the case of neutron star matter). The second reason is related with the flexibility of the slope parameter L. For finite nuclei, we consider the total energy of the nucleus in terms of an energy density functional of the proton $\rho_p(r)$ and neutron $\rho_n(r)$ number densities

$$E = \int_{\mathcal{V}} \mathcal{E}\,(\rho(r), \alpha(r))\, d^3r \tag{4}$$

where $\mathcal{E}(\rho(r), \alpha(r))$ is the local energy density, $\rho = \rho_n + \rho_p$ is the total number density and $\alpha = (\rho_n - \rho_p)/(\rho_n + \rho_p)$ is the asymmetry function. The integration is performed over the total volume $\mathcal{V}$ of the nucleus. In the present work we consider the functional

$$E = \int_{\mathcal{V}} \left(\mathcal{E}_b(\rho,\alpha) + F_o|\nabla\rho(r)|^2 + \frac{1}{4}\rho(1-a)V_C(r)\right) d^3r \tag{5}$$

where $\mathcal{E}_b$ is the energy density of asymmetric nuclear matter, the second term is the gradient term originating from the finite-size character of the density distribution and the third term is the Coulomb energy density. The minimization of the total energy, given by the functional (5), with the above constraints constitutes a variational problem. One has to solve self-consistently the system of the corresponding differential equations in order to extract the total number density $\rho(r)$. In the present work, we use a variational method where an appropriate trial function for $\rho(r)$ is used. In the present study we use a Fermi-type trial density function of the form

$$\rho(r) = \frac{\rho_0}{1 + \exp[(r-d)/w]} \tag{6}$$

One possibility is to calculate the symmetry energy coefficient a_A, defined in the Bethe-Weizsacker formula, via the local density approximation. In this approach a_A is defined by the integral

$$a_A = \frac{A}{(N-Z)^2} \int_{\mathcal{V}} \rho(r) S(\rho) \alpha^2(r) d^3r. \tag{7}$$

It was suggested that the symmetry energy coefficient a_A can be expanded as determined by the formula [18]

$$a_A^{-1} = (a_A^V)^{-1} + (a_A^S)^{-1} A^{-1/3}. \tag{8}$$

One of the most important quantities concerning the isovector character of the nuclear forces is the neutron skin thickness defined as

$$\Delta R_{\rm skin} = R_n - R_p \tag{9}$$

with

$$R_n = \left(\frac{1}{N}\int_{\mathcal{V}} r^2 \rho_n d^3r\right)^{1/2} = \left(\frac{1}{N}\int_{\mathcal{V}} r^2 \frac{\rho(1+\alpha)}{2} d^3r\right)^{1/2} \tag{10}$$

and

$$R_p = \left(\frac{1}{Z}\int_{\mathcal{V}} r^2 \rho_p d^3r\right)^{1/2} = \left(\frac{1}{Z}\int_{\mathcal{V}} r^2 \frac{\rho(1-\alpha)}{2} d^3r\right)^{1/2} \tag{11}$$

It is worth mentioning that $\Delta R_{\rm skin}$ is not directly dependent on $S(\rho)$, compared to the case of a_A.

2.2 Equation of State and Neutron Stars

The EoS of neutron star matter is the key quantity to study the structure and the properties of neutron stars [19, 20]. It consists mainly by two parts. The first one is the contribution of the baryons (neutrons and protons mainly) and the second is the contribution by leptons (mainly electrons and muons). In the present work the contribution on the energy density of neutron star matter is given by the expression (1). The pressure, due to the baryons which is defined as

$$P_b = n^2 \frac{d(\mathcal{E}/n)}{dn} \tag{12}$$

reads now

$$P_b = \frac{K_0}{9n_0^2} n^2 (n - n_0) + \alpha^2 \frac{L}{3n_0} n^2 \tag{13}$$

Having now constructed the EoS of neutron star matter we can calculate their basic properties (mass, radius and tidal deformability) by solving the Tolman-Oppenheimer-Volkoff (TOV) that express the hydrostatic equilibrium. This system reads

$$\begin{aligned} \frac{dP(r)}{dr} &= -\frac{G\mathcal{E}(r)M(r)}{c^2 r^2}\left(1 + \frac{P(r)}{\mathcal{E}(r)}\right) \\ &\times \left(1 + \frac{4\pi P(r) r^3}{M(r)c^2}\right)\left(1 - \frac{2GM(r)}{c^2 r}\right)^{-1}, \end{aligned} \tag{14}$$

$$\frac{dM(r)}{dr} = \frac{4\pi r^2}{c^2}\mathcal{E}(r). \tag{15}$$

To solve the coupled differential equations for $P(r)$ and $M(r)$, numerical integration is performed from the origin ($r = 0$) to the point where the pressure reaches zero ($r = R$). At this point, the radius and mass of the neutron star are determined.

The solving of the coupled differential equations (14) and (15) for $P(r)$ and $M(r)$ requires their numerical integration from the origin ($r = 0$) to the point $r = R$ where the pressure becomes practically zero. At this point the radius and the mass of the neutron star are computed.

In recent years, valuable information has been obtained from observations of gravitational waves resulting from mergers of black hole–neutron star and neutron star–neutron star binary systems. These sources enable the measurement of various properties of neutron stars. During the inspiral phase of binary neutron star systems, tidal effects become detectable. Specifically, the tidal Love number k_2 describes the neutron star's response to the tidal field and depends on both the neutron star mass and the applied EoS. The exact relationship describing these tidal effects is given below [21, 22]

$$Q_{ij} = -\frac{2}{3} k_2 \frac{R^5}{G} E_{ij} \equiv -\lambda E_{ij}, \tag{16}$$

where λ is the tidal deformability. The tidal Love number k_2 is given by [21, 22]

$$\begin{aligned} k_2 &= \frac{8\beta^5}{5}(1-2\beta)^2\left[2 - y_R + (y_R - 1)2\beta\right] \\ &\times \Big[\, 2\beta\left(6 - 3y_R + 3\beta(5y_R - 8)\right) \\ &+ 4\beta^3\left(13 - 11y_R + \beta(3y_R - 2) + 2\beta^2(1 + y_R)\right) \\ &+ 3(1-2\beta)^2\left[2 - y_R + 2\beta(y_R - 1)\right]\ln(1 - 2\beta)\Big]^{-1} \end{aligned}$$

where $\beta = GM/Rc^2$ is the compactness of a neutron star. The parameter y_R is determined by the following differential equation [21, 22]

$$r\frac{dy(r)}{dr} + y^2(r) + y(r)F(r) + r^2 Q(r) = 0 \tag{17}$$

$F(r)$ and $Q(r)$ are functions of the energy density $\mathcal{E}(r)$, pressure $P(r)$, and mass $M(r)$ defined as

$$F(r) = \left[1 - \frac{4\pi r^2 G}{c^4}\left(\mathcal{E}(r) - P(r)\right)\right]\left(1 - \frac{2M(r)G}{rc^2}\right)^{-1},$$

and

$$\begin{aligned} r^2 Q(r) &= \frac{4\pi r^2 G}{c^4}\left[5\mathcal{E}(r) + 9P(r) + \frac{\mathcal{E}(r) + P(r)}{\partial P(r)/\partial \mathcal{E}(r)}\right] \\ &\times \left(1 - \frac{2M(r)G}{rc^2}\right)^{-1} - 6\left(1 - \frac{2M(r)G}{rc^2}\right)^{-1} \\ &- \frac{4M^2(r)G^2}{r^2c^4}\left(1 + \frac{4\pi r^3 P(r)}{M(r)c^2}\right)^2 \\ &\times \left(1 - \frac{2M(r)G}{rc^2}\right)^{-2}. \end{aligned}$$

Eq. (17) must be solved numerically and self consistently with the TOV equations under the following boundary conditions: $y(0) = 2$, $P(0) = P_c$ (P_c denotes the central pressure), and $M(0) = 0$. The numerical integration provides the value of $y_R = y(R)$, which is a basic ingredient for k_2.

In addition, an important and well measured quantity by the gravitational wave detectors, which can be treated as a tool to impose constraints on the EoS, is the dimensionless tidal deformability Λ, defined as [21, 22]

$$\Lambda = \frac{2}{3} k_2 \left(\frac{c^2 R}{GM}\right)^5 = \frac{2}{3} k_2 (1.473)^{-5}\left(\frac{R}{\mathrm{Km}}\right)^5\left(\frac{M_\odot}{M}\right)^5 \tag{18}$$

We notice that Λ is sensitive to the neutron star radius, hence can provide information for the low density part of the EoS, which is related also to the structure and properties of finite nuclei.

3 Results and Discussion

We calculate the properties of the nucleus ^{208}Pb for various values of the parameter η including the neutron skin ΔR_{skin} and the coefficients a_A, a_A^S and a_A^V. The value of the symmetry energy at the saturation density $n_0 = 0.16$ fm^{-3} is fixed at $J = 32$ MeV. The results are presented in

Table 1. The incompressibility K_0 (in MeV), the slope parameter L (in MeV), the parameter η (in MeV), the $\Delta R_{\rm skin}$ (in fm), a_A (in MeV), a_A^S (in MeV), a_A^V (in MeV) for various equations of state.

K_0	L	η	ΔR_{skin}	a_A	a_A^S	a_A^V
220	40	70.61	0.046	27.87	35.59	32.11
224	48	80.21	0.069	26.85	27.57	32.13
228	56	89.42	0.097	25.72	21.71	32.14
232	64	98.31	0.132	24.45	17.19	32.17
236	72	106.95	0.177	22.95	13.49	32.20
240	80	115.38	0.240	21.09	10.28	32.26
244	88	123.63	0.350	18.44	7.84	30.59
248	96	131.72	0.438	14.84	6.48	24.20
252	104	139.69	0.510	10.48	4.58	17.08
256	112	147.53	0.562	5.464	2.37	8.95

Table 2. The incompressibility K_0 (in MeV), the slope parameter L (in MeV), the parameter η (in MeV), the $R_{\rm max}$ (in Km), $M_{\rm max}$ (in $M_\odot$), $R_{1.4}$ (in Km) and $\Lambda_{1.4}$ for various equations of state.

K_0	L	η	R_{max}	M_{max}	$R_{1.4}$	$\Lambda_{1.4}$
220	40	70.61	10.78	2.34	12.15	333
224	48	80.21	10.89	2.36	12.39	385
228	56	89.42	11.01	2.37	12.61	441
232	64	98.31	11.12	2.38	12.85	505
236	72	106.95	11.23	2.39	13.08	579
240	80	115.38	11.34	2.40	13.33	664
244	88	123.63	11.44	2.41	13.59	768
248	96	131.72	11.55	2.42	13.87	896
252	104	139.69	11.65	2.43	14.19	1048
256	112	147.53	11.77	2.44	14.54	1253

Table (1). The effects of the stiffness of the EoS are more pronounced in the case of the neutron skin and the coefficients a_A and a_A^S and moderately so for a_A^V. The comparison of the skin with the experimental data from PREX-2 can lead to some constraints on the parameter η. Considering that the values of the skin of ^{208}Pb reported by PREX-2 are [11, 12]

$$\Delta R_{\rm skin} = (0.283 \pm 0.071)\ {\rm fm} \tag{19}$$

where the quoted uncertainty represents a 1σ error, we conclude that the values of η are roughly limited in the interval $\eta \sim [110 - 120]$ MeV.

Moreover, in Table (2) we provide the values of the maximum mass $M_{\rm max}$ (in $M_\odot$), the corresponding radius $R_{\rm max}$ (in Km), the values of the radius $R_{1.4}$ (in Km) which correspond to mass 1.4 $M_\odot$ and finally the tidal deformability $\Lambda_{1.4}$ corresponding to mass 1.4 $M_\odot$, for each specific case.

Fig. 1 (left panel) shows the mass-radius relation for a neutron star. The EoSs, parameterized by η, are depicted with solid curves; lighter colors indicate higher η values. Shaded regions represent observational data. Higher η values correlate with increased maximum mass ($M_{\rm max}$) and radius, with the radius being more sensitive to η. EoSs with the highest η exceed the GW170817 observational limits [23], while only the lowest η value aligns with HESS observations [24].

Fig. 1 (right panel) presents the dimensionless tidal deformability as a function of neutron star mass for all considered EoSs. The green point and its error bar represent the estimated $\Lambda_{1.4}$ from the GW170817 detection [23]. Notably, EoSs with higher η values do not match the observed $\Lambda_{1.4}$.

To further examine the dependence of the EoS on the η parameter, we constructed Fig. 2 (left panel). This figure shows the tidal deformability $\Lambda_{1.4}$ of a 1.4 $M_\odot$ neutron star as a function of η. Each marker represents an EoS with a specific η value, with lighter colors indicating higher η. By applying the LIGO observational limits for $\Lambda_{1.4}$, we determined an upper value of $\eta_{\rm max} \simeq 106.676$ MeV. EoSs with $\eta \leq \eta_{\rm max}$, indicated by the orange horizontal arrows, meet the observational constraints from GW170817. The red color curve corresponds to a fitted formula, which in a good approximation is given in the following form

$$\Lambda_{1.4}(\eta) = c_1 \exp{(c_2^\eta)}, \tag{20}$$

where $c_1 \simeq 63.38614$ and $c_2 \simeq 1.00745$.

We studied the neutron skin thickness $\Delta {\rm R}_{\rm skin}$ in relation to $\Lambda_{1.4}$ to extract more information from observational constraints, as shown in Fig. 2 (middle panel). Each marker represents an EoS from the previous figure. The upper limit $\Lambda_{1.4} = 580$ sets a maximum neutron skin value of $\Delta {\rm R}_{\rm skin} = 0.175$ (green dashed line). The limits from PREX-2 translate to an acceptance region for $\Lambda_{1.4}$ between 632.379 and 777.727 (purple horizontal dashed lines). These constraints diverge: gravitational-wave data suggest smaller neutron skin values, while PREX-2 data imply larger values, reflecting the softer EoS required by GW170817 and the stiffer EoS indicated by PREX-2.

To delve deeper into the microscopic parameters, we constructed Fig. 2 (right panel). This diagram utilizes the observational upper limit of $\Lambda_{1.4} = 580$ from GW170817 (green area) to determine a lower limit for each parameter. For the surface coefficient, this limit is $\alpha_A^S \geq 13.45837$. Based on the estimated region for $\Lambda_{1.4}$ derived from PREX-2 neutron skin measurements, the surface coefficient should be within $\alpha_A^S \in [8.23576, 11.68261]$. The behavior of $\Lambda_{1.4}(\alpha_A^S)$ can be well-described by an exponential formula.

$$\Lambda_{1.4}(\alpha_A^S) = c_3 \exp(-\alpha_A^S/c_4) + c_5 \exp(-\alpha_A^S/c_6) + c_7, \tag{21}$$

where $c_3 = 1082.95$, $c_4 = 6.18075$, $c_5 = 552.26432$, $c_6 = 71.30309$, and $c_7 = 3.32712 \times 10^{-7}$. The distinct estimation values (originating from either observational data that we used) reiterate for the other two microscopic parameters, α_A and α_A^V, as one can observe from Fig. 2.

4 Concluding Remarks

The main conclusions of the present study can be summarized as follows

- The neutron skin thickness and the coefficients a_A, a_A^S, and a_A^V are sensitive to the parameter η, which charac-

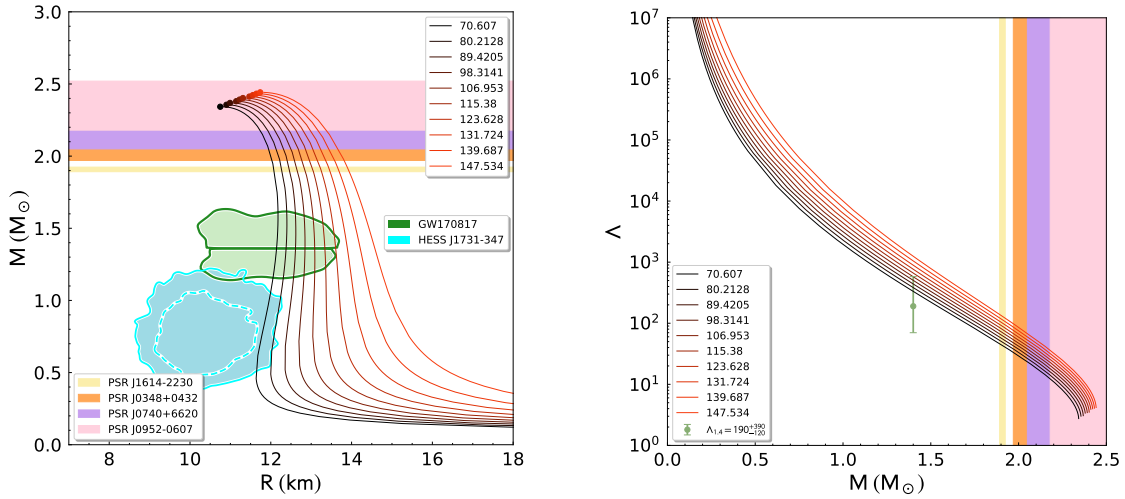

Figure 1. (left): The mass-radius (M-R) dependence for various EoSs depending on the parameter η. Various astrophysical constraints have been included for comparison (shaded regions). The shaded regions from bottom to top represent the HESS J1731-347 remnant [24], the GW170817 event [23], PSR J1614-2230 [25], PSR J0348+0432 [26], PSR J0740+6620 [27], and PSR J0952-0607 [28] pulsar observations for the possible maximum mass. (Right): The dimensional tidal deformability Λ as a function of the mass for various EoSs corresponding to the selected values of the parameter η. The shaded vertical regions indicate observational estimations as in the left panel, while the error bar indicates the estimation of Ref. [23].

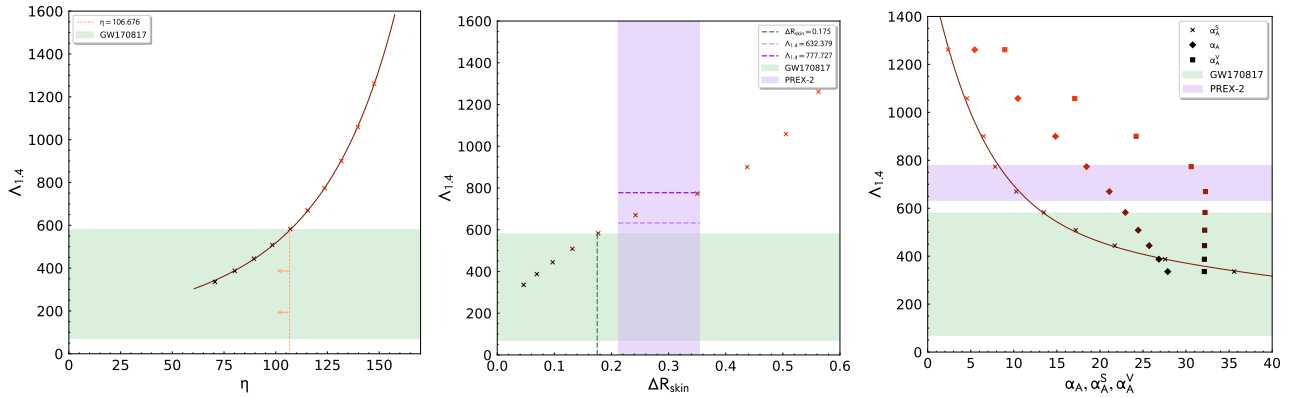

Figure 2. (Left): The tidal deformability $\Lambda_{1.4}$ of a 1.4 $M_\odot$ neutron star related to the parameter η. The green shaded area indicates the observational constraints from GW170817 [23]. (Middle): The tidal deformability $\Lambda_{1.4}$ of a 1.4 $M_\odot$ neutron star related to the neutron skin thickness ΔR_{skin} (in fm). The green shaded area indicates the observational constraints on $\Lambda_{1.4}$ by GW170817 [23], while the purple one indicates the PREX-2 estimation for ΔR_{skin} [11]. (Right): The tidal deformability $\Lambda_{1.4}$ of a 1.4 $M_\odot$ neutron star related to the asymmetry coefficient α_A (in MeV) and the surface (volume) coefficient α_A^S (α_A^V) (in MeV). The green shaded area indicates the observational constraints on $\Lambda_{1.4}$ by GW170817 [23], while the purple one indicates the corresponding PREX-2 [11] estimation for $\Lambda_{1.4}$.

terizes the stiffness of the EoS. This sensitivity is especially pronounced for high values of η ($\eta > 120$ MeV), resulting in abnormal values for these parameters.

- For the neutron skin thickness to be compatible with the results of the PREX-2 experiment, the parameter η must lie within the range 110 MeV $\lesssim \eta \lesssim$ 125 MeV.

- The influence of the parameter η is significantly noticeable in neutron star properties. Specifically, increasing η affects the radius more than M_{max}. EoSs with the highest η values fall outside the GW170817 observational bounds, while only EoSs with the lowest η values can match the HESS observations.

- Using the observational constraints of $\Lambda_{1.4}$ from LIGO, we identified an upper limit of $\eta_{max} \simeq 106.676$ MeV. This ensures that all equations of state (EoSs) with $\eta \leq \eta_{max}$ satisfy the observational constraints of GW170817.

- These two constraints, stemming from observational and experimental data, lead to divergent implications. Gravitational-wave observations suggest smaller values for the neutron skin thickness, whereas PREX-2 measurements favor higher values. This discrepancy arises from the softer EoS required by GW170817, contrasting with the stiffer EoS preferred by PREX-2.

- For the first time, we establish constraints on the three other microscopic parameters, α_A, α_A^S, and α_A^V, using recent observations primarily related to tidal deformability. Our findings suggest that refining measurements of tidal deformability, and consequently neutron star radius, will further refine the range of these coefficients.

Since the symmetry energy has been extensively discussed and utilized in this work, it is worth exploring this topic further. Most experimental data concerning symmetry energy are concentrated in the saturation density region, but there is significant uncertainty at higher densities. As a result, it is challenging to reliably fit theoretical models to the corresponding experimental values at these high densities. Consequently, extrapolation becomes inevitable, leading to considerable uncertainty regarding the plausibility of the theoretical predictions. The model proposed in this work accurately reproduces the predictions from Ref. [29], particularly when using L values in the range of 60 – 90 MeV. Lower L values result in softer equations of state, while higher L values produce stiffer equations of state. In any case, most of the predicted equations of state fall well within the experimental predictions of Ref. [29], ensuring their reliability up to twice the saturation density.

A final comment is in order: Although this study uses a simple model to simultaneously describe finite nuclei and neutron stars, the results demonstrate that despite the vast difference in their dimensions (ranging from a few femtometers to several kilometers), they can be directly connected due to the common isovector dependence of their properties. Therefore, it is reasonable to assume that future precise measurements of neutron star properties will lead to a more accurate determination of the microscopic structure of finite nuclei, particularly neutron-rich ones, and vice versa. This work is an effort in that direction.

Acknowledgments

This work is supported by the Hellenic Foundation for Research and Innovation (HFRI) under the 3rd Call for HFRI PhD Fellowships (Fellowship Number: 5657).

References

[1] M. Baldo and G.F. Burgio, Prog. Part. Nucl. Phys. **91**, 203 (2016).
[2] A. W. Steiner, M. Prakash, J. M. Lattimer, and P. J. Ellis, Phys. Rep. **411**, 325 (2005).
[3] F. Sammarruca, Int. J. Mod. Phys. E **22**, 1330031 (2013).
[4] J. M. Lattimer, Particles **6**, 30 (2023).
[5] J.M. Lattimer, Nucl. Phys. A **928**, 276 (2014).
[6] B.A. Li, À. Ramos, G. Verde and I. Vidaña, Eur. Phys. J. A **50**, 9 (2014).
[7] C. J. Horowitz, E. F. Brown, Y. Kim, W. G. Lynch, R. Michaels, A. Ono, J. Piekarewicz, M. B. Tsang, H. H. Wolter, J. Phys. G: Nucl. Part. Phys. **41**, 093001 (2014).
[8] Bao-An Li, Bao-Jun Cai, Wen-Jie Xie, and Nai-Bo Zhang, Universe **7**(6), 182 (2021).
[9] Bao-Jun Cai and Bao-An Li, Ann. of Phys. **444**, 169062 (2022).
[10] G.F. Burgio, H.-J. Schulze, I. Vidaña, and J.-B. Wei, Prog. Part. Nucl. Phys. **120**, 103879 (2021).
[11] D. Adhikari et al., preceding Letter, Phys. Rev. Lett. **126**, 172502 (2021).
[12] B.T. Reed, F. J. Fattoyev, C. J. Horowitz, and J. Piekarewicz, Rev. Lett., **126**, 17503 (2021).
[13] D. Adhikari et al. (CREX Collaboration), Phys. Rev. Lett. **129**, 042501 (2022).
[14] M. C. Papazoglou and Ch. C. Moustakidis Phys. Rev. C **90**, 014305 (2014).
[15] H. Sotani, K. Iida, K. Oyanatsu, and A. Ohnishi, Prog. Theor. Exp. Phys. **051**, E01 (2014).
[16] H. Sotani, N. Nishimura, and T. Naito, Prog. Theor. Exp. Phys. **041**, D01 (2022).
[17] M. Divaris, A. Kanakis-Pegios, and Ch. C. Moustakidis Phys. Rev. C **109**, 055805 (2024)
[18] P. Danielewicz and J. Lee, Nucl. Phys. A **922**, 1 (2014).
[19] T. Shapiro, Black Holes, White Dwarfs, and Neutron Stars: The Physics of Compact Objects, Wiley-VCH, New York,(1983).
[20] Haensel, P.; Potekhin, A.Y.; Yakovlev, D.G. *Neutron Stars 1: Equation of State and Structure*, Springer-Verlag, New York, 2007.
[21] Éanna É. Flanagan and Tanja Hinderer, Phys. Rev. D **77**, 021502(R) (2008).
[22] Tanjia Hinderer, ApJ **677**, 1216 (2008).
[23] B. P. Abbott et al., Phys. Rev. X **9**, 011001 (2019).
[24] V. Doroshenko, V. Suleimanov, G. Phlhofer, and Andrea Santangelo, Nat. Astron. **6**, 1444 (2022).
[25] Z. Arzoumanian, A. Brazier, S. Burke-Spolaor et al., Astrophys. J. Suppl. Ser. **235**, 37 (2018).
[26] J. Antoniadis, P. Freire, N. Wex et al., Science **340**, 448 (2013).
[27] H. Cromartie, E. Fonseca, S. Ransom et al., Nat. Astron. **4**, 72 (2020).
[28] R. G. Romani, D. Kandel, A. V. Filippenko, T. G. Brink, and W. Zheng, Astrophys. J. Lett. **934**, L17 (2022).
[29] P. Russotto et al., Pys. Rev. C **94**, 034608 (2016).